A Matched-filter Based Algorithm for Subcellular Classification of T-system in Cardiac Tissues

DFC, SRB, ACS, FBS, MF, WEL, and PKH

In mammalian ventricular cardiomyocytes, invaginations of the surface membrane form the transverse tubular system (T-system) which consists of transverse tubules (TTs) that align with sarcomeres and Z-lines as well as longitudinal tubules (LTs) that are present between Z-lines in some species. In many cardiac disease etiologies the T-system is perturbed, which is believed to promote spatially heterogeneous, dyssynchronous Ca^{2+} release and inefficient contraction. In general, T-system characterization approaches have been directed primarily at isolated cells and do not detect subcellular T-system heterogeneity. Here we present a matched-filter based algorithm for subcellular T-system characterization in isolated cardiomyocytes and millimeter-scale myocardial sections. The algorithm utilizes "filters" representative of TTs, LTs, and T-system absence. Application of the algorithm to cardiomyocytes isolated from rat disease models of myocardial infarction (MI), dilated cardiomyopathy induced via aortic banding (AB), and sham surgery confirmed and quantified heterogeneous T-system structure and remodeling. Cardiomyocytes from post-MI hearts exhibited increasing T-system disarray as proximity to the infarct increased. We found significant ($p<0.05$, Welch's *t*-test) increases in LT density within cardiomyocytes proximal to the infarct (12±3%, data reported as mean ± SD, n=3) vs. sham (4±2%, n=5), but not distal to the infarct (7±1%, n=3). The algorithm also detected decreases in TTs within 5° of the myocyte minor axis for isolated AB (36±9%, n=3) and MI cardiomyocytes located intermediate (37±4%, n=3) and proximal (34±4%, n=3) to the infarct vs. sham (57±12%, n=5). Application of bootstrapping to rabbit MI tissue revealed distal sections comprised 18.9±1.0% TTs while proximal sections comprised 10.1±0.8% TTs ($p<0.05$), a 46.6% decrease. The matched filter approach therefore provides a robust and scalable technique for T-system characterization from isolated cells through millimeter-scale myocardial sections.

INTRODUCTION

In ventricular cardiomyocytes, Ca^{2+}-induced-Ca^{2+}-release (CICR) begins with the propagation of an action potential along the cell membrane, eliciting sarcolemmal Ca^{2+} influx via L-type Ca^{2+} channels (LCCs). These channels are primarily localized within sarcolemma (SL) invaginations comprising the T-system.[1] Localized Ca^{2+} entry via LCCs triggers neighboring ryanodine receptors (RyRs) located in the sarcoplasmic reticulum (SR) membrane to open and release Ca^{2+} from SR stores.[1–4] The spatiotemporal synchrony and homogeneity of CICR is critical in maintaining efficacious contraction of the heart. In rabbit, canine, and human ventricular cardiomyocytes this transverse tubular system (T-system) is comprised predominantly of TTs coinciding with the Z-lines. In rodent ventricular cardiomyocytes, the T-system includes both TTs as well as significant longitudinal tubule (LT) and axial tubule components.[5,6] In failing hearts, severe morphological changes in the T-system of ventricular cardiomyocytes promotes impairment of critical excitation-contraction coupling (ECC) Ca^{2+} handling mechanisms[1,7] that drive Ca^{2+} dysregulation and cardiac dysfunction.[8–10]

Advances in fluorescence-based microscopy offer outstanding potential to probe mechanisms governing T-system remodeling. However, the nature of T-system remodeling is diverse, with some pathologies almost strictly presenting tubule absence (TA), while others can exhibit tubules in non-transverse arrangements. Among the disease models that manifest evident changes in cardiomyocyte T-system, distinctive patterns have emerged from reduced TT density in type-II diabetic mice[11] to the coupled observation of TA and increased LT density with differing patterns for congenital heart failure,[12] spontaneous hypertension/heart failure,[13] and other disorders.[14] Substantial amounts of sub-micron resolution confocal microscopic images exist for several models of heart failure (concentric hypertrophy and dilated hypertrophy, for instance) in species including mice,[9,12,15–17] rabbit,[18–20] canine,[21,22] and human.[23,24] However, quantitative assessments of subcellular T-system remodeling have been limited.

Characterization of images and correlating structural features with cardiac function[25] represent significant challenges that permit computational solutions. Several algorithms were introduced to automate the characterization of cardiomyocyte T-system. Among these approaches is the 'TT index' or 'TT power', whereby the relative spacing and angle of TT arrangements are estimated by Fourier analysis.[26,27] The TT index correlates well with the severity of remodeling, but provides limited structural classification. More recent methods apply some level of preprocessing in order to essentially increase the amplitude of the signal arising from the TTs.[26,27] The most common metric appears to be binary thresholding, which increases contrast by converting all pixels to binary values, depending on their value relative to a user-determined threshold. Others utilize morphological transformations which produce 'skeletonized' representations of the T-system which enhance the TT index.[26–28] Recent uses of techniques such as histogram equalization[29] have been tuned to improve existing analysis approaches.[26–28] The advantage of these approaches is that they assume little prior knowledge about the structure of the T-system, yet their applications have been limited to single cardiomyocyte preparations.

Here we present a matched-filter based image processing algorithm for the subcellular characterization of cardiomyocyte T-system. The method relies on user-provided images, or filters, representing features of interest, such as native TTs, LTs, and TA. In contrast to methods that binarize images to highlight features, this algorithm preserves a dynamic range of the original image. We outline the corresponding workflow in Fig. 1, which we use to characterize the total cellular content of intact TT structure, LTs, and TA in isolated sham, MI, and dilated cardiomyopathy via ascending aortic banding (AB) cells as well as MI tissue sections (cell and tissue preparation

summarized in Sect. S.2.1).

MATERIALS AND METHODS

Matched filter theory and application

Matched filtering describes a procedure for detecting a known signal, s, or in vector form, $\hat{s}$, embedded in statistically uncorrelated noise, $\hat{n}$, via the relationship

$$y = \hat{s}\mathbf{C_n}^{-1}\hat{m} \tag{1}$$

where y is the likelihood the known signal is embedded in the measured signal, $\hat{m}$ is the measured signal ($\hat{m} = \hat{s} + \hat{n}$),[30] and $\mathbf{C_n}$ is the noise covariance ($\mathbf{C_n} = \mathbb{E}[\hat{n}\hat{n}^T]$, where $\mathbb{E}[\hat{n}\hat{n}^T]$ signifies the expectation of a random, spatially distributed noise vector, $\hat{n}$). The overarching principle in matched filtering is to identify a matched filter, $\hat{h}$, that maximizes the signal-to-noise ratio for a measurement, $\hat{m}$,[30] via

$$y = \hat{h}^T\hat{m} = \hat{h}^T\hat{s} + \hat{h}^T\hat{n}, \tag{2}$$

where $\hat{h}^T$ denotes the filter's transpose. We utilize this approach in the first stage of our workflow in order to assess the likelihood that a filter representing a feature of interest is present in a given data set. Often the signal, or multiple instances thereof, is embedded within a larger data set ($\hat{r}$), such as an image. In which case, determining the location of $\hat{s}$ within $\hat{r}$ is commonly performed by convolving the filter $\hat{h}$ with the image, $\hat{r}$, via

$$Y = \hat{h} * \hat{r} \tag{3}$$

$$= \mathscr{F}_N^{-1}\left[\mathscr{F}_N[\hat{h}] \cdot \mathscr{F}_N[\hat{r}]\right], \tag{4}$$

where $Y(x, y)$ is the likelihood of finding the known signal, $\hat{s}$ in the image, $\hat{r}$ at (x, y), while $\mathscr{F}_N$ and $\mathscr{F}_N^{-1}$ represent the discrete Fourier transform and inverse Fourier transform, respectively, to solve Eq. 3 via the convolution theorem. Probable detections of the filter $\hat{h}_i$ within Y_i are then based on identifying positions at which the response is above a user-specified threshold criterion, λ_i. To classify where cellular microstructure resembles known filters, we evaluate

$$Y_i = \hat{h}_i * \hat{r}, \quad \forall\, \hat{h}_i \in \{\hat{h}_1, \hat{h}_2, ...\} \tag{5}$$

The optimal filter is chosen as $\max(\{Y_1, Y_2, ...\})$, so long as there exists at least one Y_i for which $Y_i(x, y) > \lambda_i$. Regions of the test confocal data that returned responses below the threshold parameters for all filters considered are designated as 'uncharacterized.' Matched filter data reported herein for TT, LT, and TA filters are reported as percent characterized cell area of total cell area for each filter.

Matched filter determination

Here we determine the matched filters based on manually identifying representative T-system structure in the confocal data. The three morphological characteristics that we identified were TT, LT, and TA regions. The filters are shown in Fig. S6. The TT filter consisted of two separated binary TT structural elements. The complement to this filter was utilized as a penalty filter as described in Sect. S.1.3. The LT filter consisted of a one sarcomere wide longitudinal structural element with varying intensity according to a normal distribution along the x axis. This allowed for greater specificity of LT versus TT detection by attenuating the spectral overlap of the filters. The TA filter was a sarcomere-length square smoothing filter. The presence of sub-threshold pixels in the smoothed image indicated the presence of sarcomere-sized regions of low signal density. Details for selecting optimal threshold parameters and corresponding receiver operator characteristic (ROC) curves are provided in Sect. S.3.1.

Analysis of TTs within 5° of myocyte minor axis

Because our method relies on convolution, quantification of local tubule orientation relative to the defined myocyte minor axis, termed tubule striation angle, is straightforward. Isolated cardiomyocytes and tissue sections were manually oriented via the included graphical user interface such that the observable majority of TTs were parallel to the y axis. We manually oriented the cardiomyocytes for simplicity, but in principle this process could be automated by utilizing angles inferred from the power spectral density of the low spatial frequency information of the outer SL. Filters were rotated at 5° increments, between -25° and 25°, and convolved with the image. TT filter hits at -5°, 0°, and 5° relative to the specified minor axis were compared to the total number of hits across all rotations.

Tissue section analysis

Relative to analysis of isolated cardiomyocytes, the tissue-level characterization presented unique challenges, including the overall computational burden of processing much larger datasets as well as segmenting out non-myocyte regions. To reduce computational expense, we utilized graphics processing unit (GPU)-acceleration to evaluate the Fast Fourier Transforms utilized in our matched filtering approach (see Sect. S.2.5 for more details). For the second challenge, we introduced a penalty filter to increase specificity of the TT filter in the presence of non-cardiac regions (see Sect. S.1.3 for more details). Thus, for these analyses, we did not mask the cell boundaries as done for the isolated cardiomyocytes. Given that no mask was applied to the images, we found that the performance of the LT filter was substantially degraded and thus was not included.

Computational tools

All aforementioned numerical procedures were conducted using the PYTHON2.7 libraries NUMPY, SCIPY and OPENCV-PYTHON. Data processing was performed using scipy and jupyter notebooks. All source code is provided at https://bitbucket.org/pkhlab/matchedmyo. A limited set of tests can be performed with the code at http://athena.as.uky.edu/node/7. Details of the statistical analyses, algorithm use, and algorithm refinements are provided in the supplemental methods.

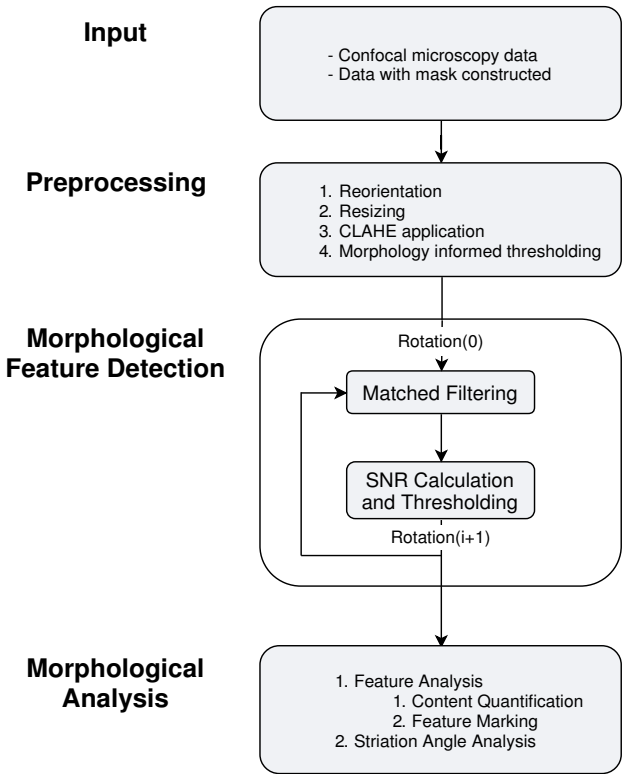

Figure 1: Unicellular matched filtering protocol. 1) Input of confocal microscopy data and user generated mask for that data. 2) Integrated preprocessing routines. 3) Morphological feature detection via matched filtering and signal-to-noise ratio calculation. 4) Morphological analysis of features, feature density, and feature rotation. A detailed version of this workflow with representative images is provided in Fig. S7.

RESULTS AND DISCUSSION

Analysis of isolated cardiomyocytes

Cardiomyocytes from sham rat model

We first demonstrate the matched filtering approach using images of sham cells (Fig. 2A), in which the TTs exhibit a regular, striated pattern (see Sect. S.2.1 for details on cell isolation and imaging). Nevertheless, subregions of the cardiomyocyte presented an appreciable degree of spatial and angular variation. In Fig. 2B, we present the classification results, for which the TT, LT, and TA responses are overlaid as blue, green, and red, respectively. In order to improve the classification results, we utilized a mask to exclude the cell membrane and nuclei in the field of view. In this image, the TT structure predominates over the LT and TA signals (Fig. 2B), which we summarize in Table S4. This difference in response is a direct result of the optimization procedure outlined in Sect. S.3.1. Finally, we present in Fig. 2C a heatmap of tubule striation angle superimposed onto the original image, where red corresponds to a TT filter hit at $-25°$ and blue corresponds to a TT filter hit at $+25°$.

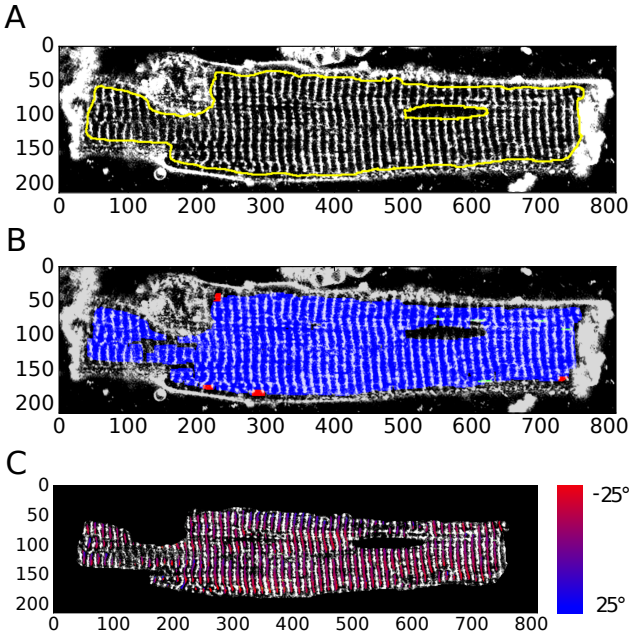

Figure 2: Algorithm application to isolated sham cells. Cardiomyocyte A) image with region of interest indicated by yellow line and B) image with transverse tubules (TT, blue), longitudinal tubles (green), and tubule-system absence (red) marked. C) indicates angle of TT relative to Y axis. Angle is denoted via a heatmap where red corresponds to a hit at the leftmost rotation angle of $-25°$ and blue corresponds to a hit at the rightmost rotation angle of $+25°$.

In principle, similar conclusions can be drawn by visual inspection of these images or application of other analyses, such as the TT index. However, one benefit of the matched-filtering approach is the ability to detect spatially heterogeneous variations in the TT structure. For instance, the TT striations are not strictly straight throughout the cardiomyocyte interior. Rather, the striations appear to accommodate roughly perpendicular orientations relative to the outer SL along the major axis. In traditional TT index or power methods, such spatial variations in angular frequencies would present a diffuse signal response in the Fourier domain, leading to a potential misclassification of subcellular structure, unless outer sarcolemma is masked or the region of interest is restricted to a small area. Because our method relies on convolution, we quantified the variation (Table S4). Here, we find that sham cells present 57±12% of striations within 5° of the myocyte minor axis (all data presented as mean ± SD, see Sect. S.2.4 for details on statistical analysis). We also note that in rodent species, the T-system presents considerable branching that manifests in significant axial contributions.[5] These features were not evident in the cells considered here owing most likely to the resolution of the microscopy data. For the LT and TA criterion, we report no significant responses in Fig. 2.

Remodeling in AB cardiomyocytes

We next investigated T-system remodeling in tissue derived from a rat model of dilated cardiomyopathy based on AB.[31] In these animals, AB emulates pressure overload, which is known to drive hypertrophic remodeling broadly throughout cardiac tissue.[32] Commonly, tissue derived from AB mice present considerable TA, which correlates with impaired contractile function.[33,34] Here we applied the algorithm to the tissue shown in Fig. 3A, using identical filters and thresholds from the previous sham analysis. As shown in Fig. 3A and Table S4, we find that TT content is significantly reduced ($p<0.05$) in AB isolated cardiomyocytes (19±14%) relative to sham (78±11%). This results in pervasive TA regions for AB cardiomyocytes (37±13%) vs. sham (9±5%). TA regions appear to be localized to the midline of the cell interior, whereas intact structure is mostly maintained adjacent to the outer plasma membrane. While TTs appear to be adjacent to the outer SL, there remains a significant ($p<0.05$) decrease in TTs within 5° of myocyte minor axis (36±9%) vs. sham. We report no significant changes in LT content for AB cardiomyocytes (5±1%) vs sham (4±2%).

Cardiomyocytes in MI rat heart

MI introduces a localized necrotic region in tissue. Cells adjacent to this necrotic region and border zone exhibit varying degrees of remodeling.[35] Here we applied the algorithm to cardiomyocytes isolated from regions distal (D, Fig. 3B), intermediate (I, Fig. 3C), and proximal (P, Fig. 3D) to an MI. These cells were obtained from an infarcted heart after explantation, for which the border zone was removed, and the remaining non-infarcted regions of the heart were divided into 3 equal-sized regions as described previously.[36] Relative to the sham cardiomyocytes, proximal cardiomyocytes exhibited a substantial increase in LTs (12±3%, $p<0.05$) as well as a

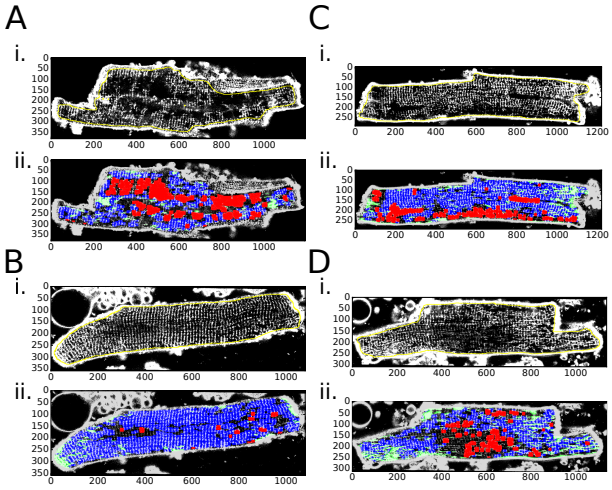

Figure 3: Algorithm application to cells isolated from rat disease models. A) Isolated cardiomyocyte from dilated cardiomyopathy model based on ascending aortic banding. B-D) Isolated cardiomyocytes from infarcted myocardium model located distal, intermediate, and proximal to the infarct, respectively. i.) Image with region of interest enclosed in yellow. ii.) Image with transverse tubules (blue), longitudinal tubules (green), and tubule absence (red) marked.

decrease in TT density, indicated by TA filter hits (12±6%, Fig. 3B-D and Table S4). Cardiomyocytes from the intermediate region presented both LTs (10±2%, $p<0.05$) and TA (10±7%), although to a lesser extent than the proximal cells (see Fig. S4 for cells considered in this study). Finally, we confirm for distally-derived tissue that for the four metrics used in this study, TT, LT, TA, and tubule striation angle, the differences observed were insignificant compared to sham cardiomyocytes. Relative to isolated cardiomyocytes from AB models, we see a substantial increase in LTs and a decreased amount of TA in MI. As with AB cardiomyocytes, a significant ($p<0.05$) decrease in the amount of TTs present within 5° of myocyte minor axis was observed in proximal tissue (34±4%) and intermediate tissue (37±4%) vs. sham. The main implication of this finding is that remodeling following MI appears to give rise to LTs and TT reorganization that is distinct from TA patterns exhibited in pressure overload models while exhibiting similar decreases in TTs within 5° of myocyte minor axis. Further, the extent of remodeling parallels distance from MI while TT density appears to have an inverse relationship with proximity to the MI.

Cardiac tissue from infarcted rabbit heart

In Fig. 4, we present results for application of the algorithm to MI tissue, which provides detail of the local tissue environment and the spatial distribution of tissue remodeling. Fig. 4A and C present tissue distal to an infarct. Fig. 4B and D present tissue proximal to the fibrous regions of an infarct. As observed previously in Fig. 3, there was a marked decrease in the TT content as the proximity to an infarct increased. Relative to the distal subsection (Fig. 4C), the proximal subsection (Fig. 4D) presented 45.8% detection with the TT filter across the same area (see Table S4). This is paralleled by an increase in TA detection, with the proximal subsection presenting 574% more TA content than the distal subsection. Statistical analysis corroborated these results, showing that distal tissue presented 18.9±1.0% TT detection and 9.5±2.0% TA detection while proximal tissue presented 10.1±0.8% TT detection and 16.0±2.0% TA detection (see Sect. S.2.4 for further details).

CONCLUSIONS

Our matched filtering-based technique complements existing computational algorithms for performing automated analyses of cardiomyocyte T-system.[26,27] This approach leverages detailed structural information for the features of interest, based on kernels reflective of TT, LT, and TA morphology. Its reliance on convolution permits localized assessments of remodeling that scale to tissue-level preparations.We found that the approach performed remarkably well across cardiomyocytes from different species, disease etiologies, and fields of view. Our results suggest that the matched filtering approach performs favorably for detecting different extents and modalities for T-system configurations in confocal-microscopic images, and reveal patterns of T-system structure unique to sham, MI, and AB cardiomyocytes. We found that the approach is robust to regional variation in subcellular structure and noise, while providing a first-of-its-kind method scalable to tissue-level imaging.

For the cardiomyocytes we considered, the approach supported prior work revealing interesting trends in regional variation of cardiomyocyte T-system, such as the heterogeneity of TT organization in sham cells, as well as intracellular remodeling that depended on the distance from MI.[36,38] We anticipate that these variations may give important clues into how cells adapt to their environment. This topic was previously explored by Guo et

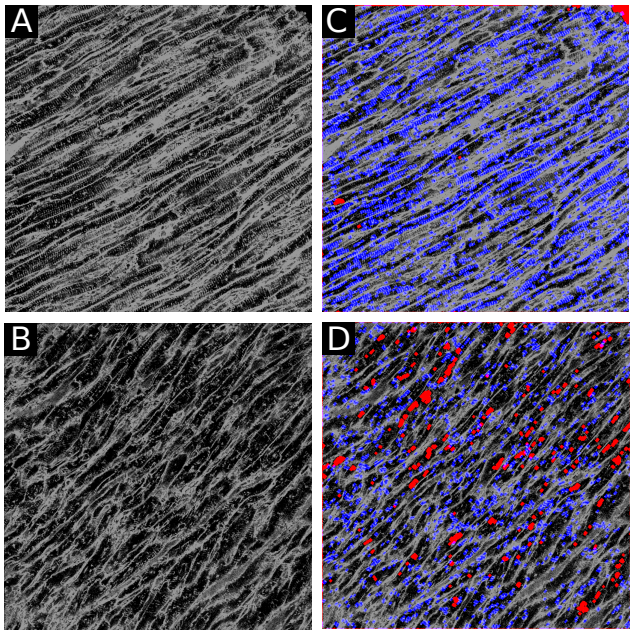

Figure 4: Application of TT filter (blue) and TA filter (red) to 3.9x4.1 mm^2 sections of infarcted rabbit tissue. A) and B) confocal images from regions distal and proximal to an infarct, respectively. C) and D) algorithm output using TT and TA filter. Striations arise from close apposition of punctate TT patterns typically observed in rabbit cardiomyocytes.[37] Relative to the distal region, the proximal region exhibited 45.8% as much TT content. Additionally, the proximal region exhibited 574% more T-system absence than the distal region.

al,[10] who cataloged diverse morphological configurations of cardiomyocyte T-system with respect to species and disease etiology.

Correlations between T-system disorganization and Ca^{2+} release dyssynchrony in numerous models of cardiac dysfunction[12,35,39,40] suggest strong linkages between cardiomyocyte remodeling and pathophysiological function. It has been observed that SL proteins can redistribute under certain conditions that correlate with Ca^{2+} mismanagement, with no observation of increased TA.[12] Accordingly, it will be invaluable to investigate the potential correlations between T-system remodeling and protein localization, as well as the extent to which those relationships influence normal physiological function. In this regard, although the data considered in this study was limited to confocal images of dye-labeled SL, it is straightforward to adapt the algorithm to diverse data sets. Hence, in the event that filters representing features of interest can be identified, the approach can be adapted to a host of different labeling and imaging techniques, as well as cells isolated from a spectrum of tissue types.

AUTHOR CONTRIBUTIONS

Following is a list of contributions made by each author. DFC: algorithm design, application/optimization of algorithm, wrote manuscript. SRB: algorithm design, edited manuscript. ACS: imaged tissue, edited manuscript. FBS: provided tools for tissue data acquisition, edited manuscript. MF: imaged isolated myocytes. WEL: provided tools for isolated myocyte data acquisition, edited manuscript. PKH: research design, algorithm design, wrote manuscript.

ACKNOWLEDGEMENTS

This work was supported by the Maximizing Investigators' Research Award (MIRA) (R35) from the National Institute of General Medical Sciences (NIGMS) of the National Institutes of Health (NIH) under grant number R35GM124977, as well as an Institutional Development Award (IDeA) from the National Institute of General Medical Sciences (NIGMS) of the National Institutes of Health (NIH) under grant number P20GM103527. We thank Mr. Noah Adler for his support in integrating our utilities onto a web platform, Darin Vaughan for critical discussion of the manuscript, and Dr. Thomas McCoy for critical description of bootstrapping techniques.

[1] D. M. Bers. *Excitation-Contraction Coupling and Cardiac Contractile Force*. Ed. by D. M. Bers. Vol. 1. Kluwer Academic Publishers: Kluwer Academic Publishers, 2001, p. 427. ISBN: 9780792371588.

[2] S. E. Litwin, J. Li, and J. H. B. Bridge. "Na-Ca Exchange and the Trigger for Sarcoplasmic Reticulum Ca Release: Studies in Adult Rabbit Ventricular Myocytes". In: *Biophysical Journal* 75.1 (July 1998), pp. 359–371. ISSN: 0006-3495.

[3] M. Stern. "Theory of excitation-contraction coupling in cardiac muscle". In: *Biophysical Journal* 63.2 (Aug. 1992), pp. 497–517. ISSN: 0006-3495.

[4] X. H. Sun et al. "Molecular architecture of membranes involved in excitation-contraction coupling of cardiac muscle." In: *The Journal of cell biology* 129.3 (May 1995), pp. 659–71. ISSN: 0021-9525.

[5] C. Soeller et al. "Examination of the transverse tubular system in living cardiac rat myocytes by 2-photon microscopy and digital image-processing techniques." In: *Circulation research* 84.3 (Feb. 1999), pp. 266–75. ISSN: 0009-7330.

[6] J. Amsellem et al. "Transverse-axial tubular system in guinea pig ventricular cardiomyocyte: 3D reconstruction, quantification and its possible role in K+ accumulation-depletion phenomenon in single cells". In: *Biology of the Cell* 85.1 (Jan. 1995), pp. 43–54. ISSN: 0248-4900.

[7] D. M. Bers. "Altered cardiac myocyte Ca regulation in heart failure." In: *Physiology (Bethesda, Md.)* 21.17 (2006), pp. 380–387. ISSN: 1548-9213.

[8] W. E. Louch, O. M. Sejersted, and F. Swift. "There Goes the Neighborhood: Pathological Alterations in T-Tubule Morphology and Consequences for Cardiomyocyte Ca2+ Handling". In: *Journal of Biomedicine and Biotechnology* 2010 (2010), pp. 1–18.

[9] W. E. Louch et al. "T tubule disorganization and reduced synchrony of Ca2+ release in murine cardiomyocytes following myocardial infarction". In: *The Journal of Physiology* 574.2 (2006), pp. 519–533.

[10] A. Guo et al. "Emerging mechanisms of T-tubule remodelling in heart failure". In: *Cardiovascular Research* 98.2 (May 2013), pp. 204–215. ISSN: 0008-6363.

[11] T. O. Stølen et al. "Interval training normalizes cardiomyocyte function, diastolic Ca2+ control, and SR Ca2+ release synchronicity in a mouse model of diabetic cardiomyopathy." In: *Circulation Research* 105.6 (2009), pp. 527–536.

[12] F. Swift et al. "Extreme sarcoplasmic reticulum volume loss and compensatory T-tubule remodeling after Serca2 knockout". In: *Proceedings of the National Academy of Sciences* 109.10 (2012), pp. 3997–4001. ISSN: 0027-8424.

[13] L.-S. Song et al. "Calcium Biology of the Transverse Tubules in Heart". In: *Annals of the New York Academy of Sciences* 1047.1 (2006), pp. 99–111.

[14] C. Ferrantini et al. "Impact of detubulation on force and kinetics of cardiac muscle contraction." In: *The Journal of general physiology* 143.6 (2014), pp. 783–97. ISSN: 1540-7748.

[15] L. Øyehaug et al. "Synchrony of Cardiomyocyte Ca2+ Release is Controlled by t-tubule Organization, SR Ca2+ Content, and Ryanodine Receptor Ca2+ Sensitivity". In: *Biophysical Journal* 104.8 (Apr. 2013), pp. 1685–1697. ISSN: 00063495.

[16] L. Li et al. "Calcium Dynamics in the Ventricular Myocytes of SERCA2 Knockout Mice: A Modeling Study". In: *Biophysical Journal* 100.2 (2011), pp. 322–331.

[17] W. E. Louch et al. "Slow Ca2+ sparks de-synchronize Ca2+ release in failing cardiomyocytes: Evidence for altered configuration of Ca2+ release units?" In: *Journal of molecular and cellular cardiology* 58 (2013), pp. 41–52.

[18] P. M. Kekenes-Huskey et al. "Modeling effects of L-type ca(2+) current and na(+)-ca(2+) exchanger on ca(2+) trigger flux in rabbit myocytes with realistic T-tubule geometries." In: *Frontiers in physiology* 3 (2012), p. 351. ISSN: 1664-042X. arXiv: PMC3463892.

[19] E. Savio-Galimberti et al. "Novel features of the rabbit transverse tubular system revealed by quantitative analysis of three-dimensional reconstructions from confocal images". In: *Biophysical Journal* 95.4 (2008), pp. 2053–2062.

[20] N. S. Torres et al. "A modified local control model for Ca2+ transients in cardiomyocytes: junctional flux is accompanied by release from adjacent non-junctional RyRs." In: *Journal of molecular and cellular cardiology* 68 (2014), pp. 1–11.

[21] H. Li et al. "Cardiac Resynchronization Therapy Reduces Subcellular Heterogeneity of Ryanodine Receptors, T-Tubules, and Ca2+ Sparks Produced by Dyssynchronous Heart Failure". In: *Circulation: Heart Failure* 8.6 (2015), pp. 1105–1114. ISSN: 19413297.

[22] F. B. Sachse et al. "Subcellular Structures and Function of Myocytes Impaired During Heart Failure Are Restored by Cardiac Resynchronization Therapy". In: *Circulation Research* 110.4 (2012), 588–U197.

[23] D. J. Crossman et al. "Changes in the organization of excitation-contraction coupling structures in failing human heart". In: *PLoS ONE* 6.3 (2011), e17901.

[24] A. R. A. R. Lyon et al. "Loss of T-tubules and other changes to surface topography in ventricular myocytes from failing human and rat heart." In: *Audio, Transactions of the IRE Professional Group on* 106.16 (2009), pp. 6854–6859.

[25] K.-L. Ang et al. "Limitations of conventional approaches to identify myocyte nuclei in histologic sections of the heart". In: *American Journal of Physiology - Cell Physiology* 298.6 (2010).

[26] C. Pasqualin et al. "Automatic quantitative analysis of t-tubule organization in cardiac myocytes using ImageJ". In: *American Journal of Physiology - Cell Physiology* 308.3 (2015), pp. C237–C245.

[27] A. Guo and L.-S. Song. "AutoTT: automated detection and analysis of T-tubule architecture in cardiomyocytes." In: *Biophysical journal* 106.12 (June 2014), pp. 2729–36. ISSN: 1542-0086.

[28] R. Arora et al. "Regional distribution of T-tubule density in left and right atria in dogs". In: *Heart Rhythm* 14.2 (2017), pp. 273–281.

[29] S. M. Pizer et al. "Adaptive histogram equalization and its variations". In: *Computer Vision, Graphics, and Image Processing* 39.3 (Sept. 1987), pp. 355–368. ISSN: 0734-189X.

[30] H. L. Van Trees. *Detection, Estimation, and Modulation Theory, Part I.* New York, USA: John Wiley & Sons, Inc., Sept. 2001, p. 716. ISBN: 0471095176.

[31] A. Feldman et al. "Selective Changes in Cardiac Gene Expression During Compensated Hypertrophy and the Transition to Cardiac Decomposition in Rats With Chronic Aortic Banding". In: *Circulation Research* 73.1 (1993), pp. 184–192.

[32] P. Jouannot and P. Hatt. "Rat myocardial mechanics during pressure-induced hypertrophy development and reversal". In: *American Journal of Physiology-Legacy Content* 229.2 (Aug. 1975), pp. 355–364.

[33] S. Wei et al. "T-tubule remodeling during transition from hypertrophy to heart failure." In: *Circulation research* 107.4 (Aug. 2010), pp. 520–31.

[34] A. R. Lyon et al. "Loss of T-tubules and other changes to surface topography in ventricular myocytes from failing human and rat heart." In: *Proceedings of the National Academy of Sciences of the United States of America* 106.16 (Apr. 2009), pp. 6854–9. ISSN: 1091-6490.

[35] W. E. Louch et al. "T-tubule disorganization and reduced synchrony of Ca2+ release in murine cardiomyocytes following myocardial infarction". In: *The Journal of Physiology* 574.2 (July 2006), pp. 519–533.

[36] M. Frisk et al. "Elevated ventricular wall stress disrupts cardiomyocyte t-tubule structure and calcium homeostasis". In: *Cardiovascular Research* 112.1 (Oct. 2016), pp. 443–451. ISSN: 0008-6363.

[37] F. B. Sachse et al. "Sub-micrometer anatomical models of the sarcolemma of cardiac myocytes based on confocal imaging". In: *Pacific Symposium on Biocomputing 2008: Kohala Coast, Hawaii, USA, 4-8 January 2008* (2008), p. 390.

[38] B. Chen et al. "β-Adrenergic receptor antagonists ameliorate myocyte T-tubule remodeling following myocardial infarction". In: *The FASEB Journal* 26.6 (June 2012), pp. 2531–2537. ISSN: 0892-6638.

[39] H. K. Mørk et al. "Slowing of cardiomyocyte Ca ¡sup¿2+¡/sup¿ release and contraction during heart failure progression in postinfarction mice". In: *American Journal of Physiology-Heart and Circulatory Physiology* 296.4 (Apr. 2009), H1069–H1079. ISSN: 0363-6135.

[40] I. Lenaerts et al. "Ultrastructural and Functional Remodeling of the Coupling Between Ca2+ Influx and Sarcoplasmic Reticulum Ca2+ Release in Right Atrial Myocytes From Experimental Persistent Atrial Fibrillation". In: *Circulation Research* 105.9 (Oct. 2009), pp. 876–885. ISSN: 0009-7330.